

## EXAFS study of hydrogen intercalation into $\text{ReO}_3$ using the evolutionary algorithm

This content has been downloaded from IOPscience. Please scroll down to see the full text.

2014 J. Phys.: Condens. Matter 26 055401

(<http://iopscience.iop.org/0953-8984/26/5/055401>)

View [the table of contents for this issue](#), or go to the [journal homepage](#) for more

Download details:

IP Address: 85.255.64.41

This content was downloaded on 16/01/2015 at 10:26

Please note that [terms and conditions apply](#).

# EXAFS study of hydrogen intercalation into $\text{ReO}_3$ using the evolutionary algorithm

J Timoshenko, A Kuzmin and J Purans

Institute of Solid State Physics, University of Latvia, Kengaraga street 8, LV-1063 Riga, Latvia

E-mail: [janis.timoshenko@gmail.com](mailto:janis.timoshenko@gmail.com), [a.kuzmin@cfi.lu.lv](mailto:a.kuzmin@cfi.lu.lv) and [purans@cfi.lu.lv](mailto:purans@cfi.lu.lv)

Received 11 November 2013, revised 5 December 2013

Accepted for publication 10 December 2013

Published 16 January 2014

## Abstract

In this study we have investigated the influence of hydrogen intercalation on the local atomic structure of rhenium trioxide using a new approach to EXAFS data analysis, based on the evolutionary algorithm (EA). The proposed EA-EXAFS method is an extension of the conventional reverse Monte Carlo approach but is computationally more efficient. It allows one to perform accurate analysis of EXAFS data from distant coordination shells, taking into account both multiple-scattering and disorder (thermal and static) effects. The power of the EA-EXAFS method is first demonstrated on an example of the model system, pure  $\text{ReO}_3$ , and then it is applied to an *in situ* study of hydrogen bronze  $\text{H}_x\text{ReO}_3$  upon hydrogen intercalation. The obtained results allow us to detect changes in the lattice dynamics and correlation of atomic motion, and to follow the structural development at different stages of the reaction.

Keywords: EXAFS, reverse Monte Carlo simulations, perovskites, phase transition,  $\text{H}_x\text{ReO}_3$

(Some figures may appear in colour only in the online journal)

## 1. Introduction

Extended x-ray absorption fine structure (EXAFS) spectroscopy is a modern method for structure analysis, which has gained in popularity during the past decades with the progress in synchrotron radiation sources [1–3]. The analysis of EXAFS data from the first coordination shell around an absorbing atom is nowadays a common tool to study the local structure of a material [4]. At the same time, modern brilliant x-ray sources allow one to record EXAFS spectra from crystalline materials with excellent quality, so that they contain contributions not only from the first, but also from significantly more distant coordination shells (up to 10 Å and further), approaching the fundamental limit set by finiteness of the effective mean free path of excited electrons [1]. Unfortunately, the presence of thermal and static disorder in the sample and the contribution of the so-called multiple-scattering (MS) effects strongly restrict the precise analysis of the total EXAFS spectrum using conventional methods [5], i.e., expanding the EXAFS spectrum in a series of contributions from distinct photoelectron paths and finding structural parameters such as average interatomic distances, coordination numbers and mean-square relative displacements

(MSRDs) using the best-fit analysis [6, 7]. Therefore, the conventional analysis beyond a few nearest coordination shells (in many cases beyond the first coordination shell only) is challenging, and a significant amount of structural information (such as distributions of bond angles, shape and orientation of coordination polyhedra, etc) often gets lost.

A good illustration of this problem is the study of the hydrogen intercalation process in crystalline  $\text{ReO}_3$ . Pure  $\text{ReO}_3$  is a simple cubic perovskite-type compound, extensively studied by the EXAFS technique in the past [8–17]. The process of the intercalation of hydrogen ions in this material was studied *in situ* in [18], and the EXAFS spectra containing contributions from atoms located at distances up to 6 Å from the absorbing rhenium atom have been obtained. At the same time, the conventional EXAFS analysis was able to provide information on the very first coordination shell around the rhenium atom only [18]. Some two-modal distribution of the Re–O distances has been observed, but it was impossible to conclude whether this complex distribution is due to a distortion of the Re–O<sub>6</sub> octahedra or to an appearance of two different types of regular octahedra [18]. Thus it is clear that structural information on the outer coordination shells and on the many atom distribution functions, which is contained in the

full EXAFS spectrum, is required to understand the influence of hydrogen intercalation on the  $\text{ReO}_3$  structure.

Several simulation-based approaches have been proposed in the past to treat this task: *ab initio* molecular dynamics [19], classical molecular dynamics (MD) [20–25], Monte Carlo (MC) [26] and reverse Monte Carlo (RMC) [27–32] methods. An *ab initio* approach is obviously extremely computationally expensive and currently can be reliably applied to investigate only small atomic clusters. The limitations of the classical MD and MC methods, in turn, are set by the fact that some effective potential functions, characterizing the interactions between atoms (the so-called force-field model), should be given, and often, especially in the case of complex structures, such functions cannot be found accurately enough. Besides, classical MD and MC methods cannot be applied to the analysis of low-temperature data due to the fact that quantum effects are neglected, while conversely the application of *ab initio* methods is usually limited to the low-temperature range.

The RMC method does not have such limitations. This method is based on the minimization of the difference between the calculated and experimentally observed structure-related properties (in our case—EXAFS spectra) of a material, simulating the atomic structure through the random displacements of atoms. Recently, we have presented the RMC implementation, designed specifically to analyze EXAFS data from crystalline materials. The proposed RMC method has been applied to study EXAFS data from crystalline germanium and crystalline rhenium trioxide  $\text{ReO}_3$  [31, 33].

While the RMC method has proved to be a valuable tool for EXAFS analysis, it is computationally inefficient. The random process that is at the heart of the RMC method usually requires many thousands of iterations until the system reaches its global minimum point. As a result, many thousands of theoretical EXAFS calculations are required, where each one of them, if all MS contributions are taken into account, may take even several minutes on modern CPUs, especially when contributions from distant coordination shells around an absorbing atom are included. Note that the calculations of theoretical EXAFS can be significantly accelerated by neglecting the dependency of the complex scattering amplitude function on interatomic distances and bonding angles, but this approach, although it is widely used in the conventional EXAFS analysis, results in small but not negligible errors. Thus, one can realize that today the feasible implementation of the RMC method is limited to the analysis of a few first-coordination shells. Moreover, the required computational time grows exponentially with an increase of the dimensionality (e.g., number of atoms) or characteristic length (e.g., the largest allowed displacements of atoms) of the configurational space over which the global minimum point is searched.

Here we propose to use the so-called evolutionary algorithm (EA) for the analysis of the total EXAFS spectra, taking into account static and thermal disorder as well as multiple-scattering effects. The EA method is an extension of the RMC algorithm and, thus, is also based on random processes. However, it turns out to be significantly more efficient in terms of the required computational power.

In this study we employ the EA method to resolve a contradiction between the results of powder neutron diffraction [34]

and x-ray absorption spectroscopy [15, 18] observed during a distortion of the local atomic structure in hydrogen rhenium bronzes  $\text{H}_x\text{ReO}_3$ .

According to a neutron diffraction study [34], the insertion of hydrogen into perovskite-type cubic  $\text{ReO}_3$  induces internal strain, which leads to a tilting and slight deformation of originally regular  $\text{ReO}_6$  octahedra and an increase of the Re–O bond lengths, while the cell volume remains almost constant. In particular, in the case of hydrogen rhenium bronze  $\text{H}_{1.36}\text{ReO}_3$ , having the largest known amount of inserted hydrogen, the Re–O–Re angles between two octahedra, determined by neutron diffraction (i.e., apparent angles [35]), change from  $\varphi_{\text{DIFFR}} = 180^\circ$  to  $169^\circ$ , the O–Re–O angles inside the octahedra become split into two groups of  $\sim 82^\circ$  and  $\sim 98^\circ$ , and the Re–O bonds lengthen by  $0.03 \text{ \AA}$  from  $\sim 1.87$  to  $\sim 1.90 \text{ \AA}$  [34].

Our previous x-ray absorption spectroscopy studies [15, 18] also indicate the occurrence of octahedra tilting upon hydrogen insertion; however, the analysis of the Re  $L_3$ -edge EXAFS suggests strong distortion of the first coordination shell of rhenium, which was tentatively interpreted as the appearance of two different rhenium sites, both having nearly regular octahedral coordination, with the Re–O bond lengths equal to  $1.88$  and  $2.06 \text{ \AA}$ , caused by the charge disproportionation phenomenon ( $2\text{Re}^{5+} \rightarrow \text{Re}^{6+} + \text{Re}^{4+}$ ). Note that the change of the rhenium formal charge seemed to be supported by a shift (about  $2 \text{ eV}$ ) of both Re  $L_1$  and  $L_3$  absorption edges [18].

Thus, the clear contradiction between the two experimental results has remained unresolved for years and will be addressed in detail below by considering both static and dynamic disorder and including correlation effects.

The paper is organized as follows: section 2 is devoted to the description of the EA-EXAFS method and the EvAX code, in which it is implemented. In section 3.1 we apply the proposed method to treat the model Re  $L_3$ -edge EXAFS for cubic  $\text{ReO}_3$ , thus illustrating the power and accuracy of the proposed approach. Next, we focus on the analysis of real experimental EXAFS data, and the effect of thermal disorder in pure cubic  $\text{ReO}_3$  before intercalation is evaluated in section 3.2. Finally, the static distortion of the  $\text{ReO}_3$  structure caused by the intercalation of hydrogen ions is studied in section 3.3. A summary of the presented results is given in section 4.

## 2. Evolutionary algorithm

### 2.1. Introduction

Evolutionary algorithm is a general name for a class of similar, population-based techniques for parameter optimization that strive to mimic genetic processes in natural systems. The most well-known type of EA is the genetic algorithm [36], for which the encoding of the variables in the form of binary strings is characteristic.

One must emphasize here, from the physical point of view the EA approach is equivalent to the well known and widely used RMC method: it is just a fitting procedure that tries to

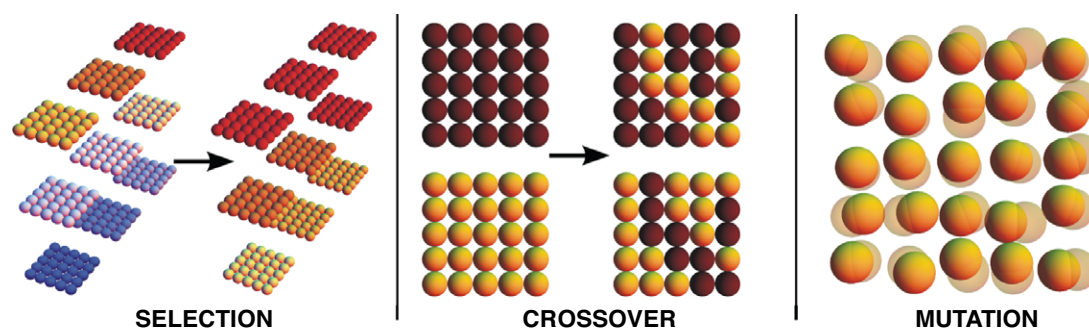


**Figure 1.** The three basic operators of the evolutionary algorithm: the selection operator chooses the best of the individuals for the next generation, keeping the total number of individuals in the population constant; the crossover operator interchanges some parts of individuals in the population, while the mutation operator applies some random changes to individuals.

find a global minimum of the system, and the same amount of information and the same constraints are used both in the RMC and EA approach. The important difference, however, is that the EA approach is much more computationally efficient. For instance, when applied to the studies of EXAFS spectra from  $\text{ReO}_3$ , we have found that using given computational power the RMC method will require probably several months to find the optimal structural model. The EA approach solved this task using the same computing resources in less than three days.

In the EA a set of current values of all parameters which should be optimized forms an ‘individual’. The function of these parameters, which needs to be maximized, is called the fitness function. The ‘population’ is an ensemble of such ‘individuals’: it consists of many sets of parameters having different values. At each iteration some manipulations with the population are carried out, so that a new population is obtained from the old one. If these manipulations, or operators, applied to the old population, are properly chosen, the fitness of the new population will be, on average, larger than for the old population. Thus, the fitness function will be maximized step by step, and the values of the parameters will approach those at the global maximum point.

In the field of structural analysis the EA has been already used, for instance, to interpret the results of powder diffraction [37, 38] and small-angle x-ray scattering [39, 40]. An interesting application of the EA is the optimization of the ground-state geometries of proteins and other large molecules [41, 42].

Nevertheless, to our knowledge, no attempts to use the EA for simulation-based interpretation of EXAFS data have been previously done. At the same time, the structure of the EXAFS spectra makes them very suitable for an analysis by EA methods: the total EXAFS spectrum can be expressed as a sum of contributions from relatively small atomic clusters, and these clusters act like the ‘genes’ of the population. The ‘genes’ that ensure high values of the fitness function survive from one generation to another, and an exchange of the ‘genes’ between individuals efficiently maximizes the fitness of each individual.

Here we apply the EA to the interpretation of EXAFS spectra from crystalline materials. In this case, the crystalline

lattice is modeled by a supercell, i.e., a sufficiently large box of atoms with periodic boundary conditions, the variable parameters are the coordinates of the atoms in the supercell, an ‘individual’ is an atomic configuration, while a ‘population’ is a set of such configurations, simulated simultaneously. For a given atomic configuration one can perform *ab initio* calculations of the configuration-averaged EXAFS spectrum, and compare the obtained theoretical result with the experimental one. The fitness function is defined so that it has its maximal value when the difference between the theoretical and experimental EXAFS spectra is the smallest. Thus, the maximization of the fitness function is equivalent to a search for the atomic configuration that represents the atomic structure of the sample and for which the theoretical EXAFS spectrum is close to the experimental one.

In the EA, three operators can usually be applied to a given population: (i) selection, (ii) crossover and (iii) mutation (figure 1). In the selection process one creates a new population (i.e., new set of atomic configurations) from the individuals of the old population, where an individual with a larger fitness function has a greater probability to get into the new population. Thus, there will be fewer atomic configurations with a low value of the fitness function in the new set, but instead there can be several copies of the atomic configurations with a high value of the fitness function. In the crossover process one replaces two randomly selected atomic configurations (‘parents’) from the old population with two other atomic configurations (‘children’), obtained by interchanging some parts of the ‘parents’, i.e., we replace some atoms of one atomic configuration with atoms of the other configuration. Finally, the mutation operator applies some small and random changes to all individuals of the population: in our case, all atoms in all configurations are slightly displaced in random directions.

These three basic operators have been implemented in the EvAX (evolutionary algorithm for XAS data analysis) code, and will be discussed below.

## 2.2. Calculation of the EXAFS spectrum

The calculation of the fitness function for an atomic configuration requires knowledge of the total theoretical EXAFS



spectrum  $\chi_{\text{tot}}(k) = \langle \chi_i(k) \rangle$ , which can be obtained by averaging the EXAFS spectra  $\chi_i(k)$ , calculated for all absorbing atoms in the supercell. *Ab initio* EXAFS calculations can be carried out by, for example, the FEFF [6] or GNXAS [43] codes. In this study, we have used the *ab initio* real-space multiple-scattering FEFF8 code [1, 6].

The EXAFS spectrum  $\chi_i(k)$  for a fixed *i*th atomic configuration is given by the equation

$$\chi_i(k) = S_0^2 \sum_j \frac{|f_j(k, \vec{r}_1, \dots, \vec{r}_m)|}{kR_j^2} \times \sin(2kR_j + \phi_j(k, \vec{r}_1, \dots, \vec{r}_m)), \quad (1)$$

where the summation is carried out over all possible scattering paths of the photoelectron (up to the eighth order in this study).  $k = \sqrt{(2m_e/\hbar^2)(E - E_0)}$  is the photoelectron wavenumber ( $m_e$  is the electron mass,  $\hbar$  is the Planck constant,  $E$  is the x-ray photon energy, and  $E_0$  is the photoelectron energy origin ( $k = 0$ )),  $S_0^2$  is the amplitude reduction factor accounting also for the multi-electron processes, and  $R_j$  is the half length of the *j*th path [1].

The complex scattering function that describes the interaction of the photoelectron with the atoms along the scattering path decomposes into the real-valued scattering amplitude  $f_j(k, \vec{r}_1, \dots, \vec{r}_m)$  and phase shift  $\phi_j(k, \vec{r}_1, \dots, \vec{r}_m)$  functions. They depend on the photoelectron energy and on both the radial and angular characteristics of the scattering path ( $\vec{r}_i$  is the position of the *i*th atom with respect to the absorbing atom), thus being responsible for the sensitivity of the total EXAFS spectrum to the 3D geometry of the scattering path.

For the calculation of the  $f_j$  and  $\phi_j$  functions in the FEFF8 code, the cluster potential is required and is constructed within the muffin-tin approximation. The complex exchange–correlation Hedin–Lundqvist potential was employed to account for inelastic losses, while the default values of muffin-tin radii, as determined within the FEFF8 code [6], were used.

The cluster potential can be either evaluated for the average atomic configuration, thus neglecting the potential variation due to thermal vibrations, or recalculated at each step. In this study, since we deal with crystalline compounds and thermal disorder is relatively low, the first approach was used and the cluster potential was evaluated before the EA-EXAFS calculations for the average crystalline structure, known from diffraction studies. This approach allowed us to reduce the total computation time significantly. It must be emphasized, however, that both functions  $f_j$  and  $\phi_j$  are recalculated at each iteration, thus their dependence on the atomic positions  $\vec{r}_i$  is taken into account explicitly.

To compare the total calculated EXAFS spectrum with the experimental one, we use the same approach as in [31]. The difference  $\xi_{k,R}$  between the theoretical and experimental EXAFS spectra is considered simultaneously in *k*- and *R*-spaces by using the so-called Morlet wavelet transform (WT) of the EXAFS spectrum [44, 45]

$$\xi_{k,R} = \frac{\|\text{WT}_{\text{tot}}(k, R) - \text{WT}_{\text{exp}}(k, R)\|_2}{\|\text{WT}_{\text{exp}}(k, R)\|_2}, \quad (2)$$

where  $\text{WT}_{\text{tot}}$  and  $\text{WT}_{\text{exp}}$  are the WTs of the calculated and experimental EXAFS spectra, respectively, and  $\|\dots\|_2$  denotes the Euclidean norm. The use of the wavelet transform allows us also to filter out the experimental noise and the contribution of outer coordination shells. Finally, the fitness function, required for the EA, is defined as  $-\xi_{k,R}$ .

When the real experimental data are treated, another problem arises besides the experimental noise: parameters  $E_0$  and  $S_0^2$  are actually unknown and their values can be different for several measurements of the same sample due to, for example, instability of the monochromator positions during the experiment. As we have already pointed out in [31], these parameters, in principle, can be refined during the EA-EXAFS simulations: in this case, the values of  $E_0$  and  $S_0^2$  are just additional variables and can be treated as all other degrees of freedom, i.e., atomic coordinates. However, such an approach is problematic due to strong correlation between  $S_0^2$  and the EXAFS amplitude, and between  $E_0$  and the EXAFS frequency. Therefore, we propose to obtain the values of  $E_0$  and  $S_0^2$  before the EA-EXAFS simulations, using conventional EXAFS analysis of the first coordination shell by, for example, the EDA [46] or ARTEMIS [47, 48], or directly FEFFIT [7] codes. The influence of uncertainty in the parameters  $E_0$  and  $S_0^2$  on the obtained results is discussed in section 3.1.

### 2.3. Selection

The selection operator can be implemented using different procedures [49, 50].

We propose to use so-called tournament selection: two atomic configurations from the old population are randomly selected (the generation of pseudo-random numbers here and further is performed using the Mersenne-Twister algorithm [51]), and the one with higher fitness is copied to the new population; the process is repeated until the number of atomic configurations in the new population is the same as in the old population [49]. The advantages of this scheme are that (i) it is very easy to implement, and (ii) it preserves the ‘genetic diversity’ of the population: the probability for the atomic configurations even with low values of fitness to be selected to the new population is still relatively large, therefore the atomic configurations in the next generation will be quite different and thus the consequent application of the selection and crossover operators will still allow one to explore configuration space efficiently.

### 2.4. Crossover

For the crossover operator we split in pairs all simulated atomic configurations in the population, which is obtained after applying the selection operator, and, then perform the ‘breeding’ of each pair with a given probability (currently a fixed value of 50% is used). First, a pseudo-random number  $\rho_b$  ( $0 \leq \rho_b \leq 1$ ) is generated. If  $\rho_b > 0.5$ , the old pair of atomic configurations (‘parents’) is replaced with a pair of new atomic configurations (‘children’). To create ‘children’, we generate a set of pseudo-random numbers  $\rho_a$  ( $0 \leq \rho_a \leq 1$ ) for each atom in the supercell of one of the parents. If  $\rho_a < 0.5$ , the corresponding atom of the first of the children is set at the same

position as the corresponding atom of the first of the parents, and the corresponding atom of the second of the children is set at the same position as the corresponding atom of the second of the parents. If  $\rho_a > 0.5$ , the interchange of atoms takes place: the corresponding atom of the first of the children is now taken from the second of the parents, and the corresponding atom of the second of the children is taken from the first of the parents.

As the crossover changes the atomic configuration, the corresponding EXAFS spectrum should be recalculated for the bred individuals. However, an advantage of the use of the crossover operator for EXAFS analysis is based on the fact that the EXAFS spectra can be expressed as a series of contributions from separate photoelectron paths, where each path contains only a few atoms. After the crossover operation some of these paths are modified, but a large number of them remain unchanged, therefore one can expect that the ‘children’ of the ‘parents’ with good fitness will also have high values of fitness function.

### 2.5. Mutation

In the conventional EA the mutation is a fully random change of the individuals, i.e., one should apply random displacements to all atoms of the population. In our approach, however, we propose to apply an additional restriction on the mutations, defined by the so-called Metropolis algorithm, thus making the EA scheme even closer to the RMC method.

Moreover, similarly to our RMC implementation [31], in the EA method we also constrain the maximal displacements of atoms from their equilibrium positions to be smaller than a given number  $\delta_{\max}$ . The equilibrium structure of crystalline materials is usually known from diffraction experiments, thus such an approach allows us to indirectly include in the EXAFS analysis the information obtained using the diffraction technique. In the case of the EA method, however, the value of  $\delta_{\max}$  is not such a crucial parameter as it was for the RMC method, and the solution can be efficiently obtained even with relatively large values of  $\delta_{\max}$ . In this study the value of  $\delta_{\max}$  was set to 0.4 Å.

Further, we will briefly recall the idea of the Metropolis algorithm. Let the differences between the total calculated and experimental EXAFS spectra for the current and new (obtained by applying mutation operator) atomic configurations be equal to  $\xi^{\text{old}}$  and  $\xi^{\text{new}}$ , respectively. According to the Metropolis algorithm [26], the criterion to accept or discard a mutation is as follows

$$\begin{aligned} &\text{if } \xi^{\text{new}} < \xi^{\text{old}}, \quad \text{the mutation is accepted} \\ &\text{if } \xi^{\text{new}} > \xi^{\text{old}}, \quad \text{the mutation is accepted, if} \\ &\exp(-(\xi^{\text{new}} - \xi^{\text{old}})/T) > \rho, \quad \text{and discarded otherwise,} \end{aligned} \quad (3)$$

where  $\rho$  is a random number in the range between 0 and 1. Such an algorithm ensures that not only mutations that improve the fitness of the atomic configurations are allowed, but also some mutations that actually decrease the value of the fitness function will be accepted, thus reducing the possibility that system gets trapped in some local minimum. As in the simulated annealing approach [52], the scaling parameter  $T$  is not fixed but decreases slowly: at the beginning of the

calculations  $T$  is large, thus a fast approach to the global minimum is ensured, but at the end of the calculations  $T$  drops to zero, and only mutations that increase the fitness of the atomic configurations are allowed.

In the EvAX code we use the same ‘cooling schedule’ (the defined time-dependency of parameter  $T$ ) as in our RMC scheme [31]

$$T(t) = -\Delta(t)/\ln(1 - t/t_{\max}), \quad (4)$$

where  $\Delta(t)$  is the average change of the difference  $|\xi^{\text{new}} - \xi^{\text{old}}|$  between theory and experiment per one mutation step, and  $t_{\max}$  is the duration of the annealing process. The cooling schedule, defined by equation (4), ensures that at the beginning of the simulation ( $t = 0$ ) all proposed mutations are accepted, after  $t = t_{\max}$  only the mutations with  $\xi^{\text{new}} < \xi^{\text{old}}$  are accepted, but in between the probability to accept a mutation with  $\xi^{\text{new}} > \xi^{\text{old}}$  changes linearly.

## 3. Application of the EA-EXAFS method

In this section we will apply the EA-EXAFS method to the EXAFS study of hydrogen intercalation into rhenium trioxide ( $\text{ReO}_3$ ). Such a complicated problem will be addressed in three steps. First, we will test the EA-EXAFS method using the simulated Re  $L_3$ -edge EXAFS spectrum of  $\text{ReO}_3$ , calculated from the classical molecular dynamics (MD) results [53] (see section 3.1). Next, the EA-EXAFS method will be applied to the analysis of the local environment around rhenium atoms upon *in situ* hydrogen intercalation. We will present and discuss the results for pure  $\text{ReO}_3$ , the starting phase, in section 3.2 and for hydrogen intercalated  $\text{H}_x\text{ReO}_3$  in section 3.3.

### 3.1. Analysis of the simulated Re $L_3$ -edge EXAFS spectrum for $\text{ReO}_3$

Before applying the EA method to experimental data, we have validated it using the simulated Re  $L_3$ -edge EXAFS spectrum for cubic  $\text{ReO}_3$ . It was obtained as a result of classical molecular dynamics (MD) calculations, and will be referred to further as the MD-EXAFS spectrum. The MD was performed for the  $5 \times 5 \times 5$  supercell with the unit cell size  $a_{\text{MD}} = 3.75$  Å in the  $NVT$  ensemble at the temperature  $T = 300$  K using the Buckingham and covalent exponential interatomic potentials to describe Re–O and O–O bonding, as described in [53]. The Re  $L_3$ -edge EXAFS spectrum has been calculated for each of the 4000 atomic configurations obtained in the MD simulations, and, finally, the configuration-averaged EXAFS spectrum (MD-EXAFS) has been obtained as the average of all these spectra (see in [53] for details). Note that the MD-EXAFS spectrum agrees well with the experimental Re  $L_3$ -edge EXAFS spectrum, measured at 300 K [53].

The EA calculations have been performed using the  $4 \times 4 \times 4$  supercell (256 atoms) by the EvAX code using different numbers of simultaneously simulated atomic configurations, but keeping the total maximal number of the calculated EXAFS spectra constant and equal to 96 000. For example, the EA calculations with 32 atomic configurations have been carried

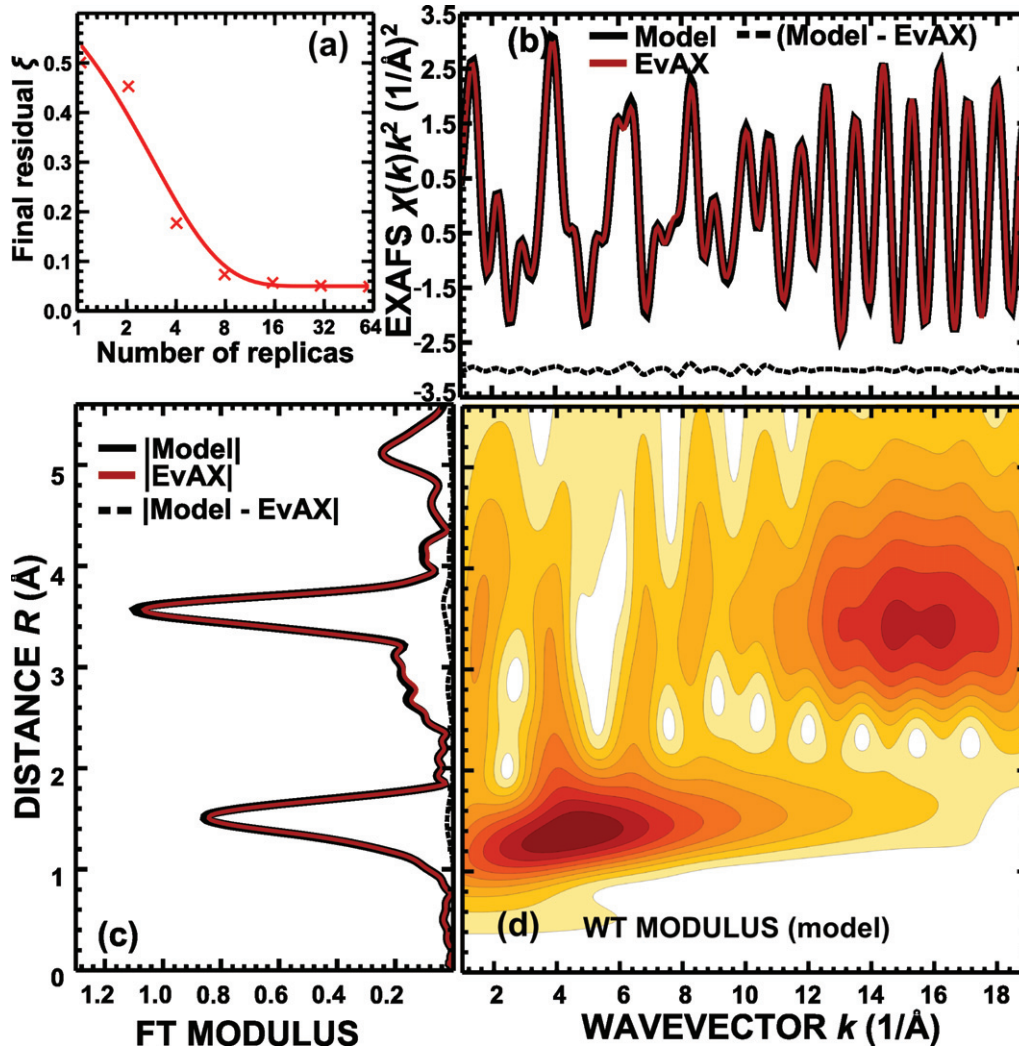


**Figure 2.** Dependence of the final difference  $\xi$  on the number of simultaneously used atomic configurations in the EA method (a). The Re  $L_3$ -edge MD-EXAFS spectrum  $\chi(k)k^2$  and the one reconstructed by the EA method using 32 atomic configurations in the population (b), their FT moduli (c), and the WT modulus of the MD-EXAFS spectrum (d).

out for 1500 iterations, so the EXAFS spectrum has been recalculated one (if only mutation operator has been applied to the given configuration) or two times (if also the crossover operator has been involved) at each iteration for each of the 32 configurations, hence the maximal number of iterations is  $32 \times 1500 \times 2 = 96\,000$ . The EA calculations with 16 atomic configurations, in turn, have been run for 3000 iterations, etc. Note that the EA calculations with only one atomic configuration are just conventional RMC calculations for 96 000 iterations, since here no selection or crossover operators can be applied.

The dependence of the final residual between the model MD-EXAFS spectrum and the one calculated by the EA method (EA-EXAFS), evaluated using equation (2), on the number of the used atomic configurations is shown in figure 2(a) (the final EA-EXAFS spectrum corresponds to one of the atomic configurations, obtained at the last iteration, which gives the best agreement between experimental and calculated EXAFS data). A comparison of the MD-EXAFS and EA-EXAFS spectra has been carried out using WT in

the  $k$ -space range from 1 to  $19 \text{ \AA}^{-1}$  and in the  $R$ -space range from 0 to  $5.6 \text{ \AA}$ , thus taking into account the contribution of the first four coordination shells around the absorbing Re atom. As one can see, the conventional RMC calculations were unsuccessful in this case: with only one atomic configuration the given number of iterations was too small, and the system got trapped in some local minimum, thus providing the largest final residual. An increase of the number of simultaneously simulated atomic configurations leads to almost exponential improvement, and already with eight atomic configurations the obtained difference between the MD-EXAFS and EA-EXAFS spectra is about six times smaller. In all further calculations we have simultaneously simulated 32 atomic configurations.

The MD-EXAFS and EA-EXAFS spectra and their Fourier transforms (FTs) are compared in figures 2(b) and (c). The EA method is able to reconstruct accurately the model data, therefore one may expect that the obtained atomic configuration should also be close to the atomic structure of the model. Here it should be emphasized that in the EA method, similarly to the conventional MC and RMC



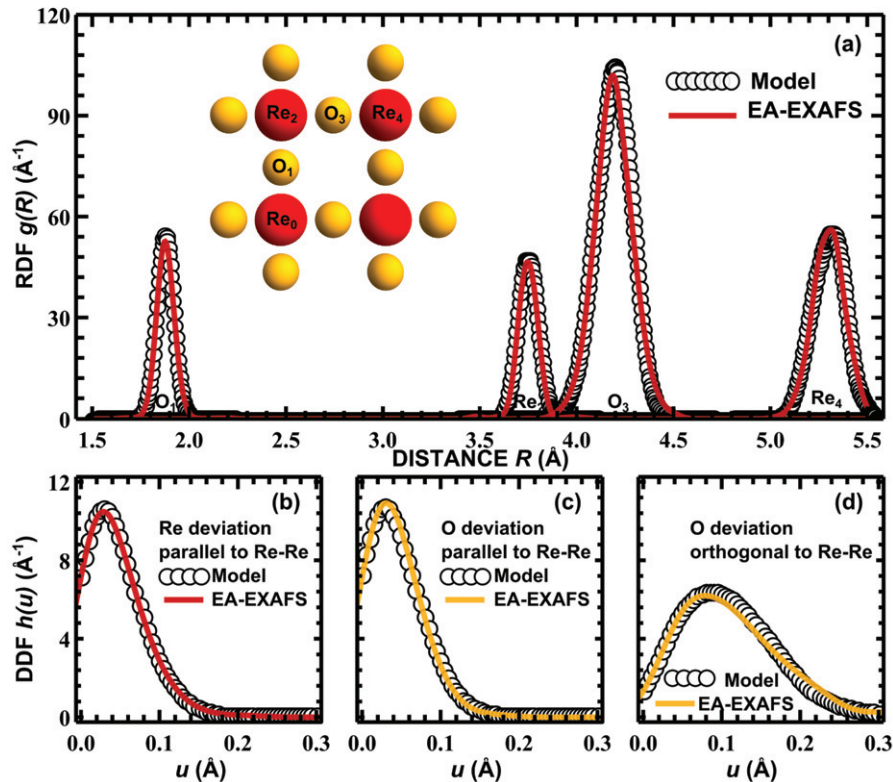


**Figure 3.** RDF around the Re atom for the first four coordination shells ( $\text{Re}_0\text{-O}_1$ ,  $\text{Re}_0\text{-Re}_2$ ,  $\text{Re}_0\text{-O}_3$ ,  $\text{Re}_0\text{-Re}_4$ , see also the inset), calculated for the MD model using the EA method (a), black solid line—RDF, obtained directly from MD coordinates; distributions of deviations of the oxygen and rhenium atoms from equilibrium positions in the direction parallel and orthogonal to the Re–Re bond, calculated using the EA method and obtained directly from MD coordinates ((b)–(d)).

methods, the obtained solution, i.e., a set of atomic positions in the configuration, is not unique. Therefore, if one repeats the simulation with a different sequence of pseudo-random numbers, another set of atomic coordinates will be obtained. However, good agreement between the obtained and model (or experimental) EXAFS spectra suggests that their statistical characteristics, such as mean values and also higher moments of interatomic distance distributions, bond-angle distributions, etc, will also be close. In fact, the radial distribution functions (RDFs) around the absorbing Re atom, calculated for our MD model and reconstructed by the EA method, are in good agreement (figure 3). Note that in this study we have used repeated EA calculations to improve the statistics; it has also allowed us later to estimate the stability of the obtained values for the structural parameters.

To make the analysis more quantitative, we have evaluated the values of average interatomic distances  $\langle R \rangle$  and variances of the distributions of interatomic distances (mean-square relative displacements, MSRDS)  $\sigma^2$ , directly calculated from the atomic coordinates for the first four coordination shells, both for the model and for the final EA configuration (see table 1). Considering the estimation of the  $\sigma^2$  parameters, one technical, but very important point is that a sample variance is a parameter that is extremely sensitive to the presence of any outliers in the sample. Therefore, while we are working with relatively small supercells, more robust estimators of  $\sigma^2$  must be used. We propose two different approaches:

(i) to use median absolute deviation (MAD) as an estimator of the MSRDS [54, 55] or (ii) to estimate the value of the MSRDS as the variance of the Gaussian function that gives the best approximation of the obtained real distribution of interatomic distances. The advantage of the MAD approach is that it can be applied even if the analyzed distribution of interatomic distances is essentially non-Gaussian. At the same time, the MAD is an inconsistent estimator, i.e., even if the analyzed population is infinitely large, the MAD estimator will not be equal to the true value of the ensemble variance. If the shape of the analyzed distribution is known then one can obtain a consistent estimator of  $\sigma$  by multiplying the MAD by some scaling constant  $K$  ( $K = 1.4826$  for Gaussian distribution [55]). The second approach, in turn, will give us a consistent estimator of the MSRDS, only if the distribution of the interatomic distances is Gaussian. Thus, the MSRDS values estimated by the second approach can be directly compared with the results obtained using conventional EXAFS analysis within the Gaussian approximation. Therefore, this second approach will be used to estimate the MSRDS values further on. Note that in all cases the same approaches have been used to estimate structural parameters both for the original MD model and for the model obtained in the EA-EXAFS simulations.

As one can see in table 1, the EA-EXAFS method gives accurate values for the average interatomic distances: the difference between the model MD data and the EA results is smaller than  $0.0025 \text{ \AA}$  for the first two coordination shells



**Table 1.** Values of the mean coordination shell radii  $\langle R \rangle$  (in Å), mean-square relative displacements (MSRDs)  $\sigma^2$  (in Å<sup>2</sup>), mean-square displacements (MSDs)  $\langle u^2 \rangle$  (in Å<sup>2</sup>), parallel ( $\cdots_{\parallel}$ ) and orthogonal ( $\cdots_{\perp}$ ) to the direction defined by the average positions of Re<sub>0</sub> and Re<sub>2</sub> atoms, and the average value of the Re<sub>0</sub>–O<sub>1</sub>–Re<sub>2</sub> angle  $\varphi_{\text{EXAFS}}$  (in °) in crystalline ReO<sub>3</sub> at 300 K for the MD model and those obtained by the EA-EXAFS simulation for the MD model (figure 2) and the experimental data (figure 4).

	EA-EXAFS results		
	MD model	MD model	Experimental data
$\langle R \rangle_{\text{Re}_0\text{--O}_1}$	1.877 4(3)	1.879(1)	1.880(1)
$\langle R \rangle_{\text{Re}_0\text{--Re}_2}$	3.748 6(5)	3.749(1)	3.749(1)
$\langle R \rangle_{\text{Re}_0\text{--O}_3}$	4.191 3(3)	4.191(1)	4.192(1)
$\langle R \rangle_{\text{Re}_0\text{--Re}_4}$	5.300 3(4)	5.300(1)	5.300(1)
$\sigma_{\text{Re}_0\text{--O}_1}^2$	0.001 05(4)	0.0011(1)	0.0026(2)
$\sigma_{\text{Re}_0\text{--Re}_2}^2$	0.001 70(6)	0.0017(1)	0.0021(1)
$\sigma_{\text{Re}_0\text{--O}_3}^2$	0.007 71(7)	0.0083(1)	0.0118(15)
$\sigma_{\text{Re}_0\text{--Re}_4}^2$	0.006 24(16)	0.0064(1)	0.0063(4)
$\langle u^2 \rangle_{\text{Re}_{\parallel}}$	0.002 5(2)	0.0027(4)	0.0033(10)
$\langle u^2 \rangle_{\text{O}_{\parallel}}$	0.002 5(2)	0.0025(2)	0.0030(2)
$\langle u^2 \rangle_{\text{O}_{\perp}}$	0.014 7(21)	0.015(1)	0.0223(59)
$\langle \varphi_{\text{EXAFS}} \rangle_{\text{Re--O--Re}}$	174.19(4)	172.8(1)	172.2(9)

and smaller than 0.005 Å for the next two coordination shells. The MSRD factors are obtained with an accuracy better than  $10^{-4}$  Å<sup>2</sup> for the first two coordination shells, and the difference of the MSRD factors for the third and fourth coordination shells is about 5%. The decrease of the accuracy for the outer shells is due to their smaller contribution to the total EXAFS spectrum relative to the first shell.

The uncertainties of structural parameters given in table 1 were estimated by comparing the results obtained in EA simulations with different sequences of pseudo-random numbers and different initial conditions, thus they reflect the statistical uncertainty of the obtained values only. For the analysis of real experimental EXAFS data one should also take into account, for instance, the influence of the uncertainty of the chosen values for the lattice constant  $a$ , and the parameters  $S_0^2$  and  $E_0$ . To estimate the importance of these effects, we have carried out additional EA-EXAFS simulations for the same MD model, but using values of  $a$ ,  $S_0^2$  and  $E_0$ , slightly different from the correct ones ( $a = a_{\text{MD}} = 3.75$  Å,  $S_0^2 = 1$  and  $E_0 = 0$  eV). The results of such calculations have shown that the errors of the obtained values of interatomic distances are very close to the error of the used value of the lattice constant. The errors of the obtained values of the MSRD factors for the first two coordination shells also depend on the error of the lattice constant and are about 0.0003 Å<sup>2</sup> for an  $a$  error equal to 0.003 Å. A 10% error in the value of the  $S_0^2$  parameter results in an approximately 0.0001 Å<sup>2</sup> error in the values of the MSRD factors for the first two coordination shells, and an approximately ten times larger error in the values of the MSRD factors for the distant coordination shells. A small (few electronvolts large) error in the value of parameter  $E_0$ , in turn, does not change the obtained values of the structural

parameters significantly (the obtained differences are smaller than the statistical uncertainty of the results).

The obtained values of structural parameters for the MD model can be compared for the first coordination shell with those calculated using conventional EXAFS analysis: the average Re<sub>0</sub>–O<sub>1</sub> distance obtained using the FEFFIT code for the model spectrum is  $\langle R \rangle_{\text{Re}_0\text{--O}_1} = 1.875 \pm 0.002$  Å and the corresponding MSRD is  $\sigma_{\text{Re}_0\text{--O}_1}^2 = 0.0010 \pm 0.0002$  Å<sup>2</sup>. As one can see, these values and their uncertainties are close to those obtained by the EA-EXAFS method.

Besides MSRDs, the EA-EXAFS method allows us to obtain the mean-square displacements (MSDs)  $\langle u^2 \rangle$ , which are inaccessible for the conventional EXAFS analysis and are usually measured by diffraction techniques [56]. The knowledge of both MSRD  $\sigma^2$  and MSD  $\langle u^2 \rangle$  quantities provides one with access to correlation effects in atomic motion, since the two parameters are related by  $\sigma^2 = \langle u_A^2 \rangle + \langle u_B^2 \rangle - 2\langle u_A u_B \rangle$ , where  $\langle u_A^2 \rangle$  and  $\langle u_B^2 \rangle$  are the corresponding MSD factors for atoms A and B, and  $\sigma^2$  is the MSRD factor for the A–B bond. The distributions of atomic displacements from equilibrium, described by the displacement distribution functions (DDFs)  $h(u)$ , are shown in figure 3. In ReO<sub>3</sub> the oscillations of oxygen atoms are essentially anisotropic. Using the EA-EXAFS method one can discriminate and separately compare the distributions of displacements parallel to the direction defined by the equilibrium positions of the Re<sub>0</sub> and Re<sub>2</sub> atoms ( $u_{\parallel}$ ), and orthogonal to it ( $u_{\perp}$ ). The quantitative values of the MSD factors  $\langle u^2 \rangle$  obtained from the MD simulations and the EA-EXAFS modeling are compared in table 1. Note that all MSD factors were calculated using the MAD approach [55], both for the original MD model and for the model obtained in the EA-EXAFS simulations. The corresponding scaling coefficients  $K_{\perp} = 1.4432$  and  $K_{\parallel} = 2.2053$  were obtained by numerical simulations, assuming that the distribution of  $u_{\perp}$  is close to the Rayleigh distribution  $h(u_{\perp}) \sim u_{\perp} \exp(-a_{\perp} u_{\perp}^2)$ ,  $u_{\perp} \geq 0$ , and the distribution of  $u_{\parallel}$  is close to  $h(u_{\parallel}) \sim \exp(-a_{\parallel} u_{\parallel}^2)$ ,  $u_{\parallel} \geq 0$ . In all cases the difference between MSD factors calculated with the EA-EXAFS method and from the MD simulations is below  $2 \times 10^{-4}$  Å<sup>2</sup>.

The EA-EXAFS provides also information on the bond angles. Let us recall that since EXAFS is sensitive to the correlated motion of atoms, a spatial and temporal average of the scattering paths within the Re<sub>0</sub>–O<sub>1</sub>–Re<sub>2</sub> atom group will always result in the mean value of the true [35] (or actual [57]) Re–O–Re angle  $\varphi_{\text{EXAFS}}$  being less than 180°, even in cubic ReO<sub>3</sub> [16]. In our case, for the MD model the value of  $\varphi_{\text{EXAFS}}$  is about 174°, and the EA-EXAFS method estimates it with an accuracy of about 1°. In contrast to EXAFS, scattering methods, being sensitive to an average of the atomic positions, will give the value of the apparent Re–O–Re angle  $\varphi_{\text{DIFFR}} = 180^\circ$  in cubic ReO<sub>3</sub>, but a smaller angle value when the static tilting of ReO<sub>6</sub> octahedra occurs.

Finally it should be mentioned, as is also in case for MSD values, that small uncertainties of the lattice constant  $a$  and the parameters  $S_0^2$  and  $E_0$  do not lead to significant changes of the obtained average values for the Re–O–Re angle (the changes of MSD and the average angle value due to these uncertainties are smaller than the statistical uncertainty).

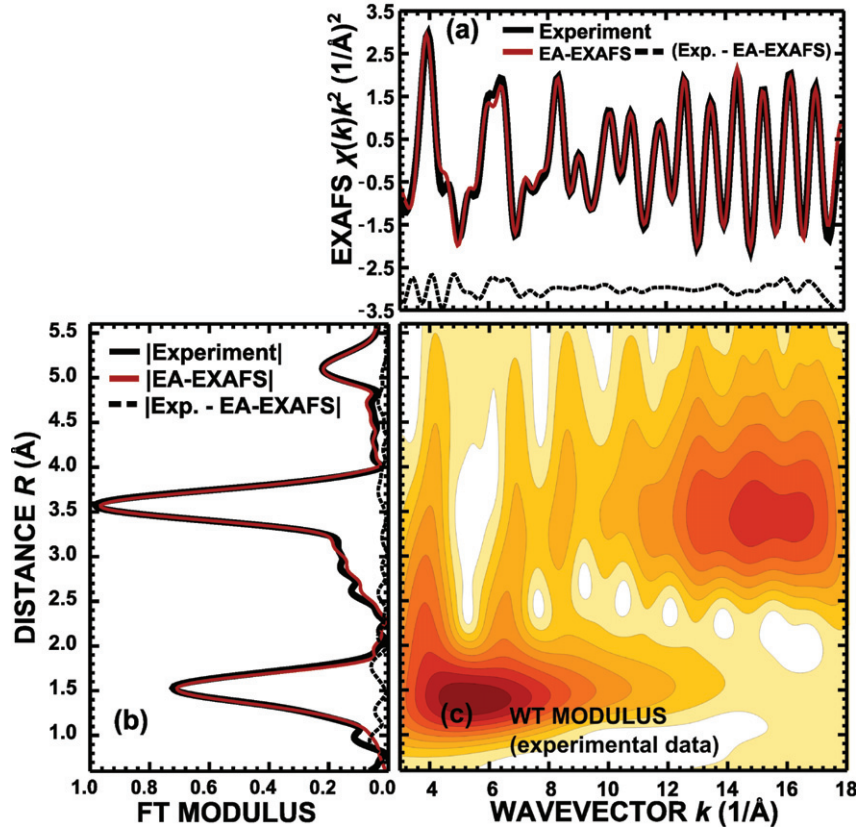


**Figure 4.** Experimental Re  $L_3$ -edge EXAFS signals  $\chi(k)k^2$  and those calculated by the EA-EXAFS method (a) and their FT moduli (b), and the WT modulus of the experimental signal (c) at  $T = 300$  K.

### 3.2. Analysis of experimental Re $L_3$ -edge EXAFS spectrum for pure $\text{ReO}_3$

In this section we apply the EA-EXAFS method to the analysis of the experimental Re  $L_3$ -edge EXAFS spectrum from cubic perovskite-type rhenium trioxide (space group  $Pm\bar{3}m$ ), measured at  $T = 300$  K [17]. The EA-EXAFS calculations were performed with 32 atomic configurations and during 1500 iterations. The lattice constant was fixed during the calculations at the experimental value  $a_{\text{ReO}_3} = 3.747$  Å [58]. The comparison of theoretical and experimental EXAFS spectra in this case has been carried out using WT in the  $k$ -space range from 3 to 18 Å<sup>-1</sup> and in the  $R$ -space range from 0.6 to 5.6 Å.

The experimental Re  $L_3$ -edge EXAFS spectra and those reconstructed by the EA method are compared in figure 4. Their good agreement is supported by their small difference  $\xi = 0.13(1)$  (see equation (2)), which is only about two times larger than in the analysis of the model MD-EXAFS spectrum.

In figure 5 we show separately the single-scattering (SS) and multiple-scattering (MS) contributions to the total EA-EXAFS spectrum. As is expected for  $\text{ReO}_3$ , the MS contribution is very important beyond the first coordination shell [10–14].

The radial distribution function (RDF) around the Re atom, calculated for the final atomic configuration, as well as the corresponding distributions of atomic displacements are compared in figure 6 and table 1 to those obtained from the MD

simulations. As one can see, the force-field model, proposed in [53], underestimates the MSRD values for the Re–O bonds, which results in the narrower RDF peaks of 1.9 and 4.0 Å. At the same time, the relative displacements of Re atoms in the second and fourth shells (peaks at 3.5 and 4.9 Å, respectively) are well reproduced. Note also that the MSRD value obtained by the EA-EXAFS analysis of experimental data for the first coordination shell agrees well with the previous results for  $\text{ReO}_3$  [13, 14].

Finally, the average value of the true Re–O–Re angle  $\varphi_{\text{EXAFS}}$  reconstructed by the EA-EXAFS method for experimental data in figure 4 is close to that found within the MD simulations (table 1). Also the apparent Re–O–Re angle  $\varphi_{\text{DIFFR}}$  is the same in both cases and is equal to 180°, supporting the conception of the cubic  $\text{ReO}_3$  structure.

### 3.3. Analysis of $\text{ReO}_3$ lattice distortion induced by intercalation of hydrogen ions

In this section we apply the EA-EXAFS method to the analysis of static disorder in the  $\text{ReO}_3$  lattice caused by intercalation of hydrogen ions. It is known that upon insertion the hydrogen ions attach to the oxygen atoms of the  $\text{ReO}_3$  lattice, forming OH bonds [34], and the valence state of formally  $\text{Re}^{6+}$  ions is reduced due to the localization of additional electrons [18]. Both effects can lead to significant distortion of the  $\text{ReO}_3$  lattice [59]. Neutron diffraction study of the hydrogen rhenium bronze  $\text{D}_{1.36}\text{ReO}_3$  has revealed that the presence of hydrogen

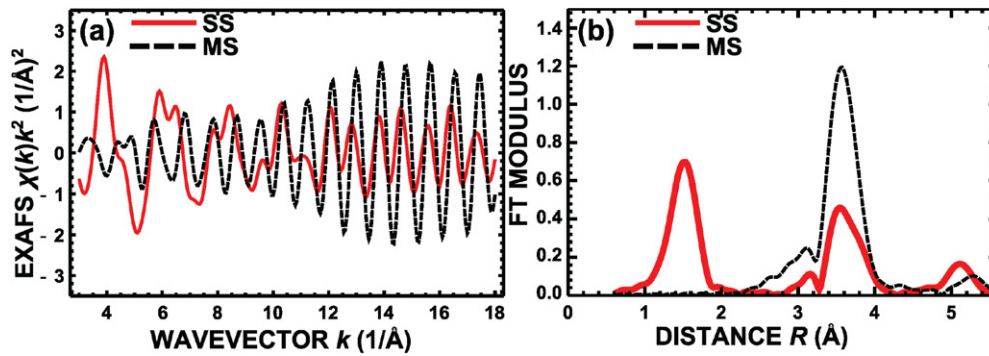


**Figure 5.** Calculated single-scattering (SS) and multiple-scattering (MS) contributions to the Re  $L_3$ -edge EA-EXAFS spectrum (a) and their Fourier transforms (b) for  $\text{ReO}_3$ .

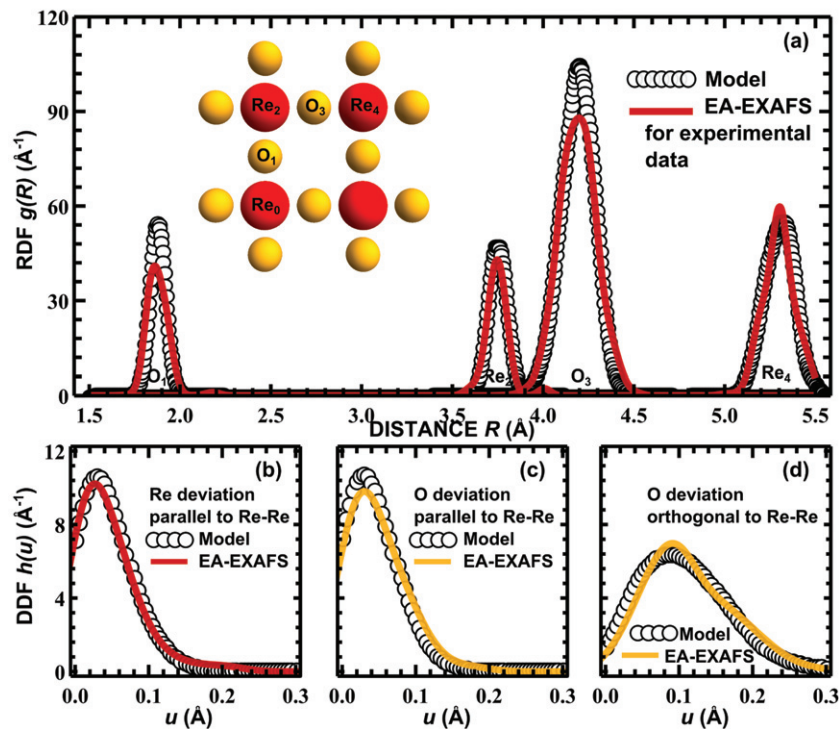


**Figure 6.** RDF around the Re atom, calculated for experimental data and RDF obtained from MD calculations (a); distributions of displacements of the oxygen and rhenium atoms from the equilibrium positions in the directions parallel and orthogonal to Re–Re bond, obtained from MD calculations and experimental data using the EvAX code ((b)–(d)).

ions leads to tilting of the  $\text{ReO}_6$  octahedra, thus significantly decreasing the average value of the apparent Re–O–Re angle  $\varphi_{\text{DIFFR}}$  [18, 34].

The experimental Re  $L_3$ -edge EXAFS data were taken from [18], where the experimental details are also given. Briefly, platinumized polycrystalline  $\text{ReO}_3$  has been exposed to hydrogen flow for 2.5 h at room temperature. Next, the air flow was passed through the sample to oxidize it and to de-intercalate the hydrogen ions. The EXAFS spectra have been *in situ* measured before the intercalation process, after the intercalation process and continuously during the de-intercalation phase.

The analysis of EXAFS spectra for pure crystalline  $\text{ReO}_3$ , for  $\text{ReO}_3$  after 2.5 h in  $\text{H}_2$  atmosphere and during the deintercalation process has been carried out using the

EA-EXAFS method with the same parameters as previously: development of 32 atomic configurations was simulated for 1500 iterations, with the lattice constant fixed during the calculations at the experimental value  $a_{\text{ReO}_3} = 3.747 \text{ \AA}$  [58]. The comparison of the experimental and calculated spectra has been carried out using WT in the  $k$ -space range from 3 to  $15 \text{ \AA}^{-1}$  and in the  $R$ -space range from 0.6 to  $5.6 \text{ \AA}$ . In the calculations we also assume that the presence of hydrogen ions itself does not have any direct contribution to EXAFS [60], and all observed changes are due to static and thermal distortions of the lattice.

The Fourier filtered experimental EXAFS spectra and those reconstructed by the EA-EXAFS method are shown in figure 7. As one can see, the disorder induced by the presence of hydrogen ions significantly reduces the amplitude of the



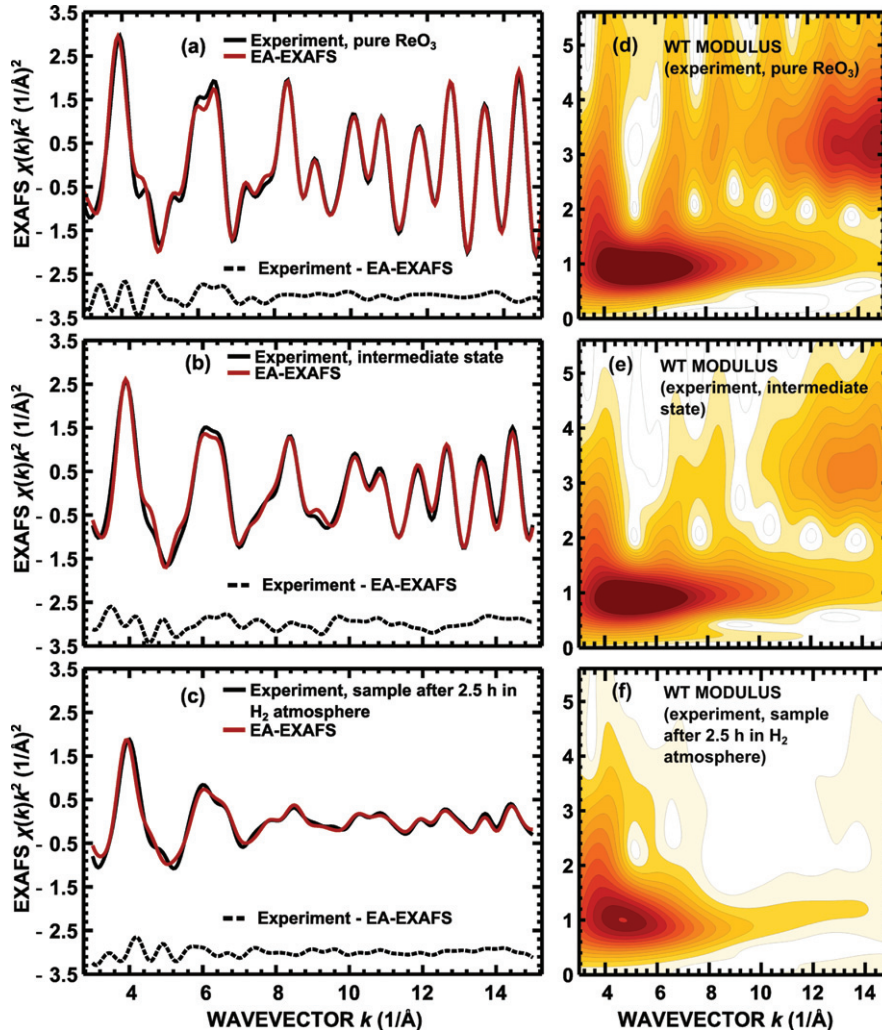


**Figure 7.** Experimental Re  $L_3$ -edge EXAFS signals  $\chi(k)k^2$  and those calculated by the EA-EWAFS method ((a)–(c)) and the WT moduli of experimental signals ((d)–(f)) for pure crystalline ReO<sub>3</sub>, for ReO<sub>3</sub> after 2.5 h in the H<sub>2</sub> atmosphere and for the intermediate state.

EXAFS spectra, so that the contribution of the second and further coordination shells to the total spectrum becomes very small after exposure to the hydrogen atmosphere for 2.5 h. Nevertheless, the EA simulations allow us to obtain structure models for which the theoretical EXAFS is reasonably close to the experimental spectra.

The RDFs around rhenium and DDFs for rhenium and oxygen, calculated from the atomic coordinates obtained in the EA simulations, are shown in figure 8. Corresponding MSRD factors for the first four coordination shells and the values of the MSD factors for rhenium and oxygen atoms, parallel and orthogonal to the direction defined by the average positions of Re<sub>0</sub> and Re<sub>2</sub>, are given in figure 9. The bond-angle distribution functions (BADF) for the true Re–O–Re angle  $\varphi_{\text{EXAFS}}$  and their mean values are shown in figure 10.

In pure ReO<sub>3</sub> the MSRD Re<sub>0</sub>–O<sub>3</sub> for the third coordination shell is large, being several times larger than the corresponding MSRD factors of the first (O<sub>1</sub>) and second (Re<sub>2</sub>) coordination shells, and also is about twice as large as the MSRD factor of the fourth (Re<sub>4</sub>) coordination shell. The large values of the MSRD factor for the Re<sub>0</sub>–O<sub>3</sub> pair can

be explained by (i) the large amplitude of oxygen oscillations in the direction orthogonal to the Re<sub>0</sub>–Re<sub>2</sub> bond, and (ii) the relatively weak correlation of motion for Re<sub>0</sub> and O<sub>3</sub> atoms. One can estimate that the correlation effects in the Re<sub>0</sub>–O<sub>3</sub> pair vibrations are negligible, since the MSRD factor  $\sigma_{\text{Re}_0\text{--O}_3}^2$  (figure 9) is close to the sum of the MSD factors for the two atoms  $\bar{\sigma}_{\text{Re}_0\text{--O}_3}^2 = \langle u_{\text{Re}}^2 \rangle + \langle u_{\text{O}_\perp}^2 \rangle / 2 \approx 0.013 \text{ \AA}^2$ .

As one may expect, the presence of hydrogen significantly broadens all peaks of the RDF, DDF and BDF, indicating the occurrence of pronounced disorder in the lattice. The average value of the true Re–O–Re angle  $\varphi_{\text{EXAFS}}$  decreases from about 172° for pure ReO<sub>3</sub> to 168° for the hydrogen intercalated H<sub>x</sub>ReO<sub>3</sub>. We have also evaluated the average value of the apparent Re–O–Re angle  $\varphi_{\text{DIFFR}}$ , which decreases from 180° to about 168° indicating a rotation of ReO<sub>6</sub> octahedra in agreement with a previous neutron diffraction study [34]. The MSRD factor (0.036 Å<sup>2</sup>) for the Re<sub>0</sub>–Re<sub>2</sub> pair increases by almost 20 times in H<sub>x</sub>ReO<sub>3</sub> relative to that (0.0021 Å<sup>2</sup>) in pure ReO<sub>3</sub>. The most significant contribution to the increase of MSRD is attributed to the reduction of the correlation between the motion of two neighboring rhenium atoms. To estimate the



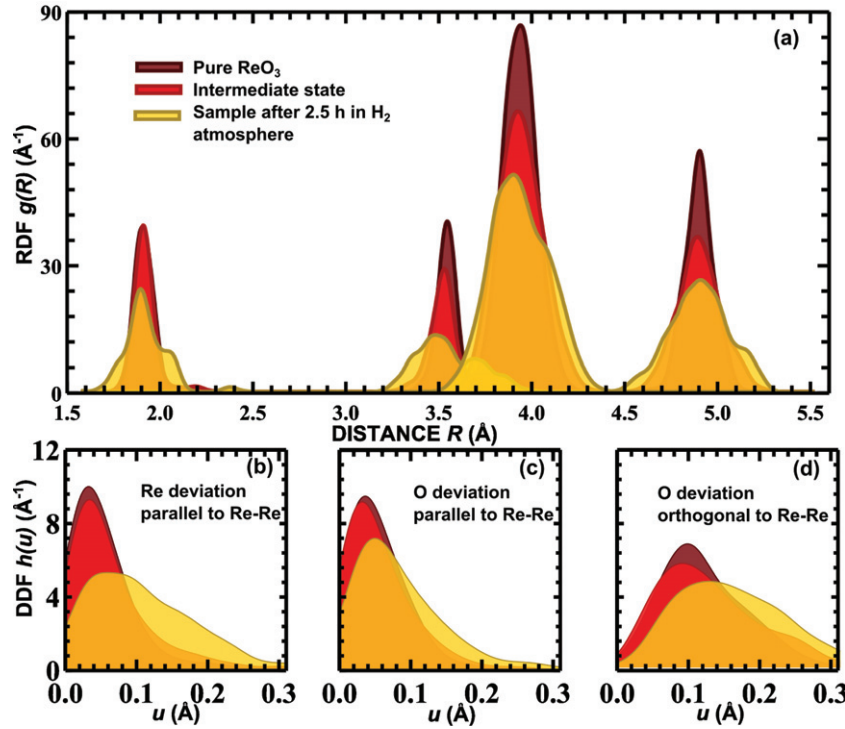


**Figure 8.** RDFs around the Re atom, calculated for pure crystalline ReO<sub>3</sub>, for ReO<sub>3</sub> after 2.5 h in the H<sub>2</sub> atmosphere and for the intermediate state (a), and corresponding distributions of the deviations of the oxygen and rhenium atoms from the equilibrium positions in the directions parallel and orthogonal to the Re–Re bond, calculated using the EA method ((b)–(d)).

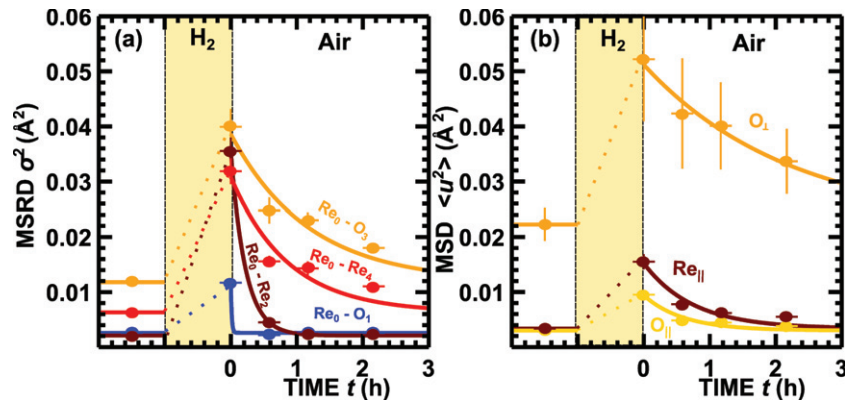


**Figure 9.** Changes of the MSRDS, calculated for experimental data for the first four coordination shells (a), and MSD factors for the displacements of Re and O atoms in the directions parallel ( $\cdot \cdot \parallel$ ) and orthogonal ( $\cdot \cdot \perp$ ) to the direction, defined by the average positions of Re<sub>0</sub> and Re<sub>2</sub>, (b) in the intercalation/de-intercalation process.

correlation effect, one again can compare the MSRDS factor  $\sigma_{\text{Re}_0-\text{Re}_2}^2$  for the second coordination shell with a sum of the MSD factors for rhenium atoms, equal to  $\tilde{\sigma}_{\text{Re}_0-\text{Re}_2}^2 = 2\langle u_{\text{Re}}^2 \rangle \approx 0.0066 \text{ \AA}^2$  for pure ReO<sub>3</sub> and  $\approx 0.031 \text{ \AA}^2$  for H<sub>x</sub>ReO<sub>3</sub>. The latter value for H<sub>x</sub>ReO<sub>3</sub> is close to the actual value of the MSRDS factor (0.036 Å<sup>2</sup>), whereas  $\tilde{\sigma}_{\text{Re}_0-\text{Re}_2}^2$  for pure ReO<sub>3</sub> is about three times larger than the actual value of  $\sigma_{\text{Re}_0-\text{Re}_2}^2 = 0.0021 \text{ \AA}^2$ . Thus, the motion of two neighboring rhenium atoms is strongly correlated in pure ReO<sub>3</sub>, whereas it is mostly uncorrelated in H<sub>x</sub>ReO<sub>3</sub>.

After the sample is exposed to air, the structural parameters gradually return to the values characteristic for pure ReO<sub>3</sub>.

One can roughly approximate these trends with exponential functions  $f(t) = f_{\text{pure}} + a \exp^{-t/\tau}$  (solid lines in figures 9 and 10), where  $f_{\text{pure}}$  is the value of the corresponding structural parameter (MSD, MSRDS or mean Re–O–Re angle),  $a$  is a free parameter,  $t$  is the experimental time, and  $\tau$  is the characteristic relaxation time. One can notice that the times  $\tau$  differ significantly for different coordination shells. In particular, the values of  $\tau$  for the MSD and MSRDS factors for the third (O<sub>3</sub>) and fourth (Re<sub>4</sub>) coordination shells, having weak correlation of atomic motion with the absorbing rhenium atom, are in the range from 0.7 to 2.5 h. In contrast, the values of  $\tau$  for the MSRDS factors for the first two coordination shells, which are

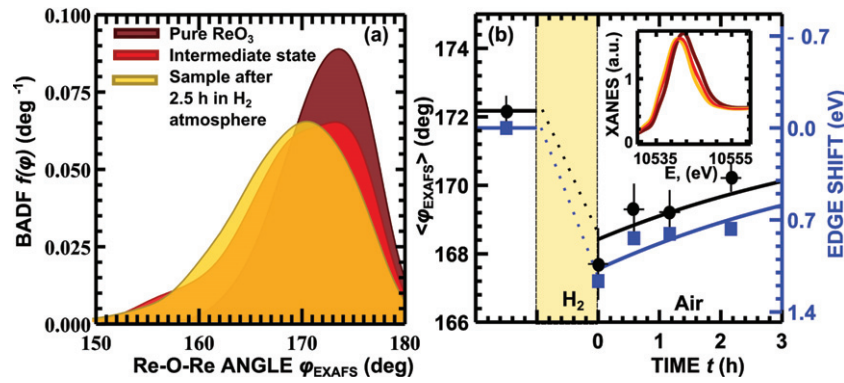


**Figure 10.** (a) Bond-angle distribution function (BADF) for the true Re–O–Re angle  $\varphi_{\text{EXAFS}}$ , calculated using the EA method for pure crystalline ReO<sub>3</sub>, for ReO<sub>3</sub> after 2.5 h in the H<sub>2</sub> atmosphere and for the intermediate state. (b) The corresponding changes of the average value of the true Re–O–Re angle in the intercalation/deintercalation process that correlate with the shift (blue squares) of the L<sub>3</sub> edge (shown in the inset).

strongly influenced by the correlation of atomic motion, are much smaller, being about 0.16 h for the MSRD of the second (Re<sub>2</sub>) coordination shell and even smaller (0.01 h) for the first (O<sub>1</sub>) coordination shell. We propose that such a difference in the characteristic relaxation times is due to the fact that the changes of the structural parameters in both of these sets have different physical origin. The changes of correlation of atomic motion and, correspondingly, of MSRD factors in the first two coordination shells have an electronic origin and, thus, short relaxation times. They arise due to additional electrons localized largely at rhenium atoms and introduced together with hydrogen ions to maintain charge neutrality. In contrast, the variation of the MSD and MSRD parameters in the third and fourth coordination shells reflects static disorder caused by the presence of hydrogen atoms in the ReO<sub>3</sub> lattice.

Finally, we will discuss the type of static disorder in the ReO<sub>3</sub> lattice induced by hydrogen insertion. Since in hydrogen rhenium bronze HReO<sub>3</sub> the formal valence state of rhenium atoms is +5, two different models for the possible lattice distortion have been proposed in [18]: (i) the distortion of all Re<sup>5+</sup>O<sub>6</sub> octahedra and (ii) the co-existence of two different types of relatively regular octahedra (Re<sup>4+</sup>O<sub>6</sub> and Re<sup>6+</sup>O<sub>6</sub>) due to the presence of two different valence states of rhenium atoms (the so-called charge disproportionation model).

To characterize the distortion of the ReO<sub>6</sub> octahedra, as well as the distortion of the octahedra formed by six Re<sub>2</sub> atoms of the second coordination shell, we used the approach proposed in [61]. For each octahedron we calculated its volume  $V_O$  and the volume  $V_S$  of the sphere that is the closest to all vertices of that octahedron. In the case of a regular octahedron such a sphere is a circumscribed sphere, and the ratio  $V_O/V_S$  is equal to  $\pi$ . The histograms of the quantity  $V_O/V_S - \pi$  for both ReO<sub>6</sub> and Re(Re<sub>2</sub>)<sub>6</sub> octahedra are shown in figure 11. They all have a single peak shape, independently of hydrogen intercalation, therefore one may conclude that only one type of rhenium–oxygen octahedra is present, thus being favorable to the first model in [18]. The broadening of the histogram peak indicates that the distortion of the ReO<sub>6</sub> octahedra increases significantly with an increase of the amount of hydrogen ions in the lattice.

Upon hydrogen insertion, the valence state of rhenium ions is reduced, which agrees with the Re L<sub>1</sub> and L<sub>3</sub> absorption edge shift by about 2 eV to smaller energies (figure 10) [18]. Therefore, the origin of the ReO<sub>6</sub> octahedra distortion can be tentatively attributed to a change of the rhenium electronic structure.

At the same time, the Re(Re<sub>2</sub>)<sub>6</sub> octahedra do not distort, although it was pointed out that the MSRD factor  $\sigma_{\text{Re}_0-\text{Re}_2}^2$  for the second coordination shell increases significantly upon hydrogen intercalation. In fact, the histograms in figure 11 are narrow, and the ratio  $V_O/V_S$  is close to  $\pi$ . It reflects the fact that, as was mentioned, the change of the value of the MSRD factor  $\sigma_{\text{Re}_0-\text{Re}_2}^2$  is mostly due to the reduction of the correlation of atomic motion, not due to static lattice distortion. This result agrees with the cubic symmetry of hydrogen rhenium bronze [34].

#### 4. Conclusions

In this study the use of a novel simulation approach, based on the evolutionary algorithm (EA), allowed us to follow structure development at different steps of hydrogen intercalation into ReO<sub>3</sub> from *in situ* EXAFS measurements at the Re L<sub>3</sub>-edge.

The EA-EXAFS method proved to be computationally more efficient than the conventional reverse Monte Carlo approach and allowed us to extract accurate structural information both from the nearest and distant coordination shells of rhenium. The obtained structural models were reconstructed, taking into account multiple-scattering and disorder (thermal and static) effects as well as the behavior of EXAFS spectra in  $k$ - and  $R$ -spaces through the use of the Morlet wavelet transform as a criterion for the residual minimization between the experimental and calculated EXAFS data.

As a result of the EA simulations, the radial distribution functions, the displacement distribution functions and the bond-angle distribution functions were obtained. The use of robust estimators allowed us to follow the variation of MSD and MSRD as functions of the de-intercalation time and to determine the characteristic relaxation times for the structural parameters in each coordination shell.

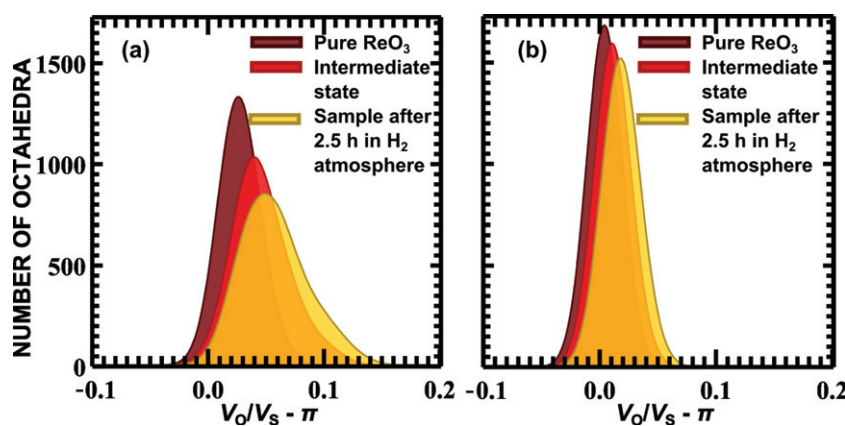


**Figure 11.** Histograms of the ratio of octahedron volume and the volume of the corresponding circumscribing sphere  $V_O/V_S - \pi$ , characterizing the distortion of the  $\text{ReO}_6$  (a) and  $\text{Re}(\text{Re}_2)_6$  (b) octahedra for pure  $\text{ReO}_3$ , for  $\text{ReO}_3$  after 2.5 h in the  $\text{H}_2$  atmosphere and for the intermediate state.

We found that atomic motion is strongly correlated in the first and second coordination shells of rhenium in cubic  $\text{ReO}_3$ , whereas it becomes significantly less correlated in  $\text{H}_x\text{ReO}_3$ . The changes in the correlation of atomic motion are attributed to an electronic origin, since they have a short relaxation time. This effect has been related to additional electrons, localized largely at rhenium atoms and entering into the crystal lattice together with hydrogen ions to maintain charge neutrality.

Besides, the insertion of hydrogen atoms leads to a distortion and tilting of the rhenium–oxygen octahedra. Our analysis revealed that these processes have significantly longer characteristic times.

To conclude, the use of such advanced simulation-based techniques as the EA-EXAFS method extends the potentiality of EXAFS spectroscopy and opens new possibilities for structure determination not accessible by conventional approaches.

## Acknowledgments

This work was supported by ESF Project 2009/0138/1DP/1.1.2.1.2/09/IPIA/VIAA/004 ('Support for Doctoral Studies at University of Latvia') and Latvian Science Council Grants Nos 187/2012 and 402/2012.

## References

- [1] Rehr J J and Albers R C 2000 *Rev. Mod. Phys.* **72** 621
- [2] Aksenov V, Kovalchuk M, Kuzmin A, Purans Y and Tyutyunnikov S 2006 *Crystallogr. Rep.* **51** 908
- [3] Yano J and Yachandra V K 2009 *Photosynth. Res.* **102** 241
- [4] Teo B 1986 *EXAFS: Basic Principles and Data Analysis* (Berlin: Springer)
- [5] Provost K, Beret E, Muller D, Marcos E S and Michalowicz A 2013 *J. Phys.: Conf. Ser.* **430** 012015
- [6] Ankudinov A L, Ravel B, Rehr J J and Conradson S D 1998 *Phys. Rev. B* **58** 7565
- [7] Newville M, Ravel B, Haskel D, Rehr J, Stern E and Yacoby Y 1995 *Physica B* **208** 154
- [8] Alberding N, Crozier E D, Ingalls R and Houser B 1986 *J. Physique* **47** 681
- [9] Vedrinskii R V, Bugaev L A and Levin I G 1988 *Phys. Status Solidi b* **150** 307
- [10] Kuzmin A, Purans J, Benfatto M and Natoli C R 1993 *Phys. Rev. B* **47** 2480
- [11] Kuzmin A and Purans J 1993 *J. Phys.: Condens. Matter* **5** 267
- [12] Houser B, Ingalls R and Rehr J J 1995 *Physica B* **208/209** 323
- [13] Dalba G, Fornasini P, Kuzmin A, Purans J and Rocca F 1995 *J. Phys.: Condens. Matter* **7** 1199
- [14] Kuzmin A, Purans J, Dalba G, Fornasini P and Rocca F 1996 *J. Phys.: Condens. Matter* **8** 9083
- [15] Purans J, Kuzmin A, Parent P and Laffon C 1999 *Physica B* **259–261** 1157
- [16] Houser B and Ingalls R 2000 *Phys. Rev. B* **61** 6515
- [17] Purans J, Dalba G, Fornasini P, Kuzmin A, Panfilis S D and Rocca F 2007 *AIP Conf. Proc.* **882** 422
- [18] Gaidelene J, Kuzmin A, Purans J and Guéry C 2005 *Phys. Status Solidi c* **2** 149
- [19] Yancey D F, Chill S T, Zhang L, Frenkel A I, Henkelman G and Crooks R M 2013 *Chem. Sci.* **4** 2912
- [20] Okamoto Y 2004 *Nucl. Instrum. Methods Phys. Res. A* **526** 572
- [21] Ferlat G, Soetens J C, Miguel A S and Bopp P A 2005 *J. Phys.: Condens. Matter* **17** S145
- [22] Kuzmin A and Evarestov R 2009 *J. Phys.: Condens. Matter* **21** 055401
- [23] Anspoks A, Kuzmin A, Kalinko A and Timoshenko J 2010 *Solid State Commun.* **150** 2270
- [24] Timoshenko J, Kuzmin A and Purans J 2011 *Cent. Eur. J. Phys.* **9** 710
- [25] Price S W T, Zonias N, Skylaris C K, Hyde T I, Ravel B and Russell A E 2012 *Phys. Rev. B* **85** 075439
- [26] Metropolis N, Rosenbluth A W, Rosenbluth M N, Teller A H and Teller E 1953 *J. Chem. Phys.* **21** 1087
- [27] McGreevy R and Pusztai L 1988 *Mol. Simul.* **1** 359
- [28] Gurman S J and McGreevy R L 1990 *J. Phys.: Condens. Matter* **2** 9463
- [29] McGreevy R L and Zetterstr P 2001 *J. Non-Cryst. Solids* **293–295** 297
- [30] McGreevy R L 2001 *J. Phys.: Condens. Matter* **13** R877
- [31] Timoshenko J, Kuzmin A and Purans J 2012 *Comput. Phys. Commun.* **183** 1237
- [32] Levin I, Krayzman V and Woicik J C 2013 *Appl. Phys. Lett.* **102** 162906
- [33] Timoshenko J, Kuzmin A and Purans J 2013 *J. Phys.: Conf. Ser.* **430** 012012
- [34] Dickens P G and Weller M T 1983 *J. Solid State Chem.* **48** 407

- [35] Barrera G D, Bruno J A O, Barron T H K and Allan N L 2005 *J. Phys.: Condens. Matter* **17** R217
- [36] Holland J 1992 *Adaptation in Natural and Artificial Systems: An Introductory Analysis with Applications to Biology, Control, and Artificial Intelligence* (Cambridge, MA: MIT Press)
- [37] Shankland K, David W and Csoka T 1997 *Z. Kristallogr.* **212** 550
- [38] Kariuki B, Serrano-González H, Johnston R and Harris K 1997 *Chem. Phys. Lett.* **280** 189
- [39] Chacón P, Diaz J, Morán F and Andreu J 2000 *J. Mol. Biol.* **299** 1289
- [40] Chacon P, Moran F, Diaz J, Pantos E and Andreu J 1998 *Biophys. J.* **74** 2760
- [41] Xiao Y and Williams D 1993 *Chem. Phys. Lett.* **215** 17
- [42] Deaven D M and Ho K M 1995 *Phys. Rev. Lett.* **75** 288
- [43] Filipponi A, Di Cicco A and Natoli C R 1995 *Phys. Rev. B* **52** 15122
- [44] Timoshenko J and Kuzmin A 2009 *Comput. Phys. Commun.* **180** 920
- [45] Muñoz M, Argoul P and Farges F 2003 *Am. Mineral.* **88** 694
- [46] Kuzmin A 1995 *Physica B* **208/209** 175
- [47] Ravel B and Newville M 2005 *J. Synchrotron Radiat.* **12** 537
- [48] Newville M 2001 *J. Synchrotron Radiat.* **8** 322
- [49] Thierens D and Goldberg D 1994 *Lect. Notes Comput. Sci.* **866** 119
- [50] Blickle T and Thiele L 1996 *Evol. Comput.* **4** 361
- [51] Matsumoto M and Nishimura T 1998 *ACM Trans. Model. Comput. Simul.* **8** 3
- [52] Kirkpatrick S, Gelatt C D and Vecchi M P 1983 *Science* **220** 671
- [53] Kalinko A, Evarestov R A, Kuzmin A and Purans J 2009 *J. Phys.: Conf. Ser.* **190** 012080
- [54] Hampel F 1973 *Probab. Theory Relat. Field* **27** 87
- [55] Daszykowski M, Kaczmarek K, Vander Heyden Y and Walczak B 2007 *Chemometr. Intell. Lab. Syst.* **85** 203
- [56] Trueblood K N, Bürgi H B, Burzlaff H, Dunitz J D, Gramaccioni C M, Schulz H H, Shmueli U and Abrahams S C 1996 *Acta Crystallogr. A* **52** 770
- [57] Tucker M G, Dove M T and Keen D A 2000 *J. Phys.: Condens. Matter* **12** L425
- [58] Chatterji T, Henry P F, Mittal R and Chaplot S L 2008 *Phys. Rev. B* **78** 134105
- [59] Hanawa M, Muraoka Y, Tayama T, Sakakibara T, Yamaura J and Hiroi Z 2001 *Phys. Rev. Lett.* **87** 187001
- [60] Lengeler B 1984 *Phys. Rev. Lett.* **53** 74
- [61] Makovicky E and Balić-Žunić T 1998 *Acta Crystallogr. B* **54** 766